ACS OMEGA

Article

Cite This: ACS Omega 2019, 4, 10388−10395

http://pubs.acs.org/journal/acsodf

Interaction of Copper Phthalocyanine with Nitrogen Dioxide and Ammonia Investigation Using X-ray Absorption Spectroscopy and Chemiresistive Gas Measurements

Liping Sharon Chia,[†,‡] Yong Hua Du,[§] Suresh Palale,[†] and Pooi See Lee*[,‡]

[†]Research and Technology Center (Asia Pacific), Corporate Research, Robert Bosch (SEA) Pte Ltd, 11 Bishan Street 21, 573943, Singapore

[‡]School of Materials Science and Engineering, Nanyang Technological University, Singapore 639798, Singapore

[§]Institute of Chemical and Engineering Sciences, Agency for Science, Technology and Research in Singapore (A*STAR), 1 Pesek Road, Jurong Island, 627833, Singapore

Supporting Information

ABSTRACT: The interaction site of phthalocyanine (Pc) with nitrogen dioxide (NO_2) has been characterized using different methods and found to be conflicting. By knowing the interaction site, the Pc molecule can be better customized to improve the gas sensitivity. In this article, the interaction sites of copper phthalocyanine (CuPc) with oxidizing NO_2 or with reducing gas (ammonia, NH_3) were identified using in situ X-ray absorption spectroscopy (XAS). The sensitivity of CuPc to sub-ppm levels of the tested gases was established in the CuPc chemoresistive gas sensors. The analyte−sensor interaction sites were identified and validated by monitoring the Cu K-edge XAS before and during gas exposure. From the X-ray absorption near-edge structure and its first derivative, a low or lack of axial coordination on the Cu metal center of CuPc is evident. Using the extended X-ray absorption fine structure with molecular orbital information of the involved molecules, the macrocycle interaction between CuPc and NO_2 or NH_3 was proposed to be the dominant sensing mechanism on CuPc sensors.

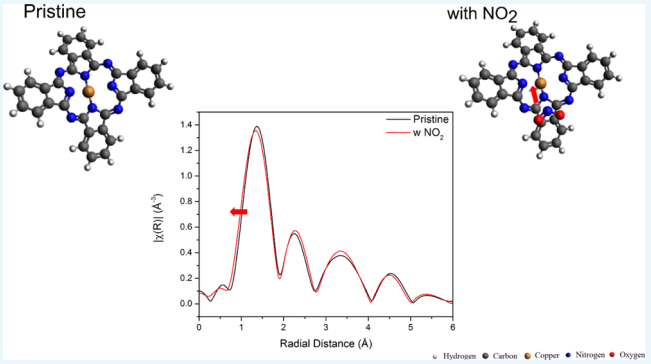

INTRODUCTION

The study of the gas composition in our environment has propelled gas sensor research for health and safety purposes, such as workplace safety in industries such as chemical and mining, as well as air-quality monitoring. One commonly researched gas analytes is nitrogen dioxide (NO_2), an oxidizing gas, which is a byproduct formed from the combustion of different forms of fossil fuels in industries, power plants, vehicles, and at home.[1,2] Another byproduct from this fossil fuel combustion is nitric oxide (NO) which oxidizes to form NO_2 in ambient environment.[3] As such, the ambient air typically contains NO_2 and NO, which are typically classified as NO_x. NO_x poses health risks by affecting the lung functions of individuals, especially in asthmatic individuals even at sub-ppm concentrations.[1,3−5] In addition, NO_x is a component of acid rain as well as of smog and air pollution, thereby leading to environmental problems.[2−4] Consequently, apart from taking measures to reduce the production of NO_x, the World Health Organization (WHO) recommends a 1 h guideline of 100 ppb,[1] whereas the National Institute for Occupational Safety and Health (NIOSH) has a recommended exposure limit (REL) of 1 ppm[6] for individuals to reduce the risk on their health. Another target gas analyte for sensors is ammonia (NH_3), which has seen an increase in its concentration in the environment over the years because of agriculture and use of fertilizers.[7−9] At low ppm levels, the alkaline reducing gas NH_3 can cause irritation to the eyes and breathing pathways.[9] Apart from posing health issues, NH_3 can also indirectly pose a threat to the environment through its redox reaction in soil to form nitrous oxide, a greenhouse gas.[10] In addition to the impact on the environment, both NO_x and NH_3 have also been found in human exhaled breath at sub-ppm levels, where an increase in concentration has been used as an indication of health or disease.[8,11]

In view of the applications of the gases at different concentrations, much research efforts have been focusing on sensors with high sensitivity to target concentrations with low cross-sensitivity to other gases. Although high sensitivity to low gas concentrations have been reported, the challenge lies in achieving high selectivity. Various gas-sensitive materials have been explored and reported, ranging from inorganic metal oxide (MO_x) to organic compounds and polymers. For

Received: August 20, 2018
Accepted: December 4, 2018
Published: June 17, 2019

DOI: 10.1021/acsomega.8b02108
ACS Omega 2019, 4, 10388−10395

miniaturized sensors, the state-of-the-art material is MO_x, such as indium oxide, zinc oxide, tungsten oxide, and tin oxide, for NO_2 or NH_3 sensing.[8,12−16] Sensors based on MO_x typically require an additional heater, as the optimum operating temperature requires hundreds of degree celsius.[12,13,15,17] Recent efforts on MO_x look into lowering this temperature requirement by making use of nanostructures, thinner films, or hybrid materials.[17−19] Alternatively, organic materials such as carbon nanotube,[20−22] pentacene,[23,24] polyaniline,[23,25,26] poly-3-hexylthiophene (P3HT),[23,24] and metal phthalocyanines (MPcs)[23,27−30] have demonstrated sensitivity to various gases, as well as room-temperature sensing. Although MO_x has the advantage of higher response than organic materials, the possibility for room-temperature sensing and higher selectivity by substituting various side groups or metal centers makes organic-sensing materials attractive.[27,30] Consequently, one such class of organic materials that have been investigated for gas-sensing purposes is MPc. MPc is a semiconducting material because of its 18π delocalized electrons in the Pc macrocycle with a thermal stability up to hundreds of degree celsius.[29] As a result, MPc has been used for sensing in conductivity-based devices. In addition, this usually thermally evaporated material can be deposited using solution process after substitution of side groups into the Pc macrocycle, thereby leading to fabrication flexibility.[30,31] On top of this, the metal center of MPc can be substituted with most of the metals in the periodic table,[29] thus making the study of MPc for sensing purposes interesting and necessary.

Apart from investigating the material's gas sensitivity and the effect of different structural properties (i.e., morphology), one other focus is to understand its analyte−sensor interaction sites. Most studies have mainly concentrated on non-substituted MPc first-row transition metal such as copper phthalocyanine (CuPc).[28,30,32] Pertaining to CuPc, the interaction with the electron-accepting gas should be located on the macrocycle based on theoretical calculations by Liao and Scheiner.[32] This is supported by the optical characterization work done by Basova et al. using Fourier transform infrared spectroscopy and Raman spectroscopy to determine the interaction mechanism with NO_2 and NH_3,[33] in which a macrocycle interaction was reported between CuPc with NO_2, whereas a metal center interaction is proposed with NH_3. On the contrary, works by Lozzi et al. suggested metal-center interaction of CuPc with NO_2.[34] As such, more comprehensive and deterministic studies should be pursued to establish a thorough understanding. In this work, X-ray absorption spectroscopy (XAS) is used to characterize the interaction sites to fully understand the sensing mechanism of the gas sensors. In situ or operando XAS studies have been utilized for various characterization work to obtain real-time process information or mechanism by looking into the changes of the target atom's coordination environment or oxidation state.[35,36] Consequently, this makes in situ characterization work using XAS with gas dosing, a direct method for analyzing CuPc that has a single Cu atom surrounded by the Pc macrocycle, despite which low dose or gas concentration would pose a challenge to this characterization method.

In this work, in situ XAS study was carried out with NO_2 or NH_3 dosing, and the interaction sites between the respective gas and CuPc layer were established. We tested the CuPc chemiresistor for sub-ppm levels of NO_2 and NH_3 sensing, and the responses of CuPc devices were also analyzed.

EXPERIMENTAL SECTION

CuPc Deposition and Chemiresistor Fabrication. Sublimed grade CuPc of 99% purity was purchased from Sigma-Aldrich and thermally evaporated on cleaned silicon substrate insulated with silicon oxide at a pressure of 3×10^{-6} mbar and a rate of 0.5 Å/s via Lesker evaporator. For gas measurements, 100 nm CuPc layer was deposited on top of 6 pairs of interdigitated Au electrodes with 0.1 mm channel length thermally evaporated at similar pressure with a rate of 1 Å/s via Mbraun evaporator. Quartz crystal microbalance in the respective equipment is used to ensure the layer thickness, which is checked using surface profiler after deposition.

Layer and Sensor Characterization. X-ray diffraction (XRD) and atomic force microscopy (AFM) were performed on the deposited CuPc on silicon substrates using Bruker ADVANCE D8 and Asylum Research Cypher S, respectively. Cu Kα X-ray (λ = 1.5406 Å) was operated at 40 kV and 40 mA for the XRD measurement, which was taken between 5° and 30° in steps of 0.018°. The CuPc layer was scanned using the AFM to obtain 1.5×1.5 μm^2 images using tapping mode with a scan rate of 1 Hz and processed using Gwyddion software.

The CuPc chemiresistor sensitivity to NO_2 or NH_3 was characterized using a Keithley 2636 with 5 V applied bias as the chemiresistor was exposed to two cycles of 50−500 ppb dry NO_2 or 0.5−2 ppm NH_3 with balance dry air consisting of 20% O_2 content at room temperature with no applied heat. Mass flow controllers (MFCs) from Bronkhorst and automatic valves were connected to a programmable logic controller (PLC) and the testing protocol was written to a program control via Labview. In this case, we are able to repeat the gas experiment easily and accurately based on the set point and duration indicated for each component. CuPc chemiresistor was dosed to each gas concentration for 60 s, whereas the recovery in dry air lasted for 120 s. Prior to the response calculation, the second cycle was first considered and the current was normalized to the start of the second cycle. The response was then calculated based on the difference in the normalized current before and after gas dosing; that is, response [gas, x ppb] = $I_{Norm,60s} - I_{Norm,0s}$. To obtain the sensitivity of the chemiresistor to NO_2 or NH_3, the response was plotted against concentration, and the sensitivity was found from the gradient of the linear fit. To prevent cross-contamination, pristine chemiresistors were used to characterize the target gas and repeated with fresh samples for reproducibility.

In Situ XAS Measurement. Cu K-edge XAS measurement of 200 nm CuPc was taken at the XAFCA beamline facility in Singapore Synchrotron Light Source (SSLS)[37] in fluorescence mode at room temperature with no vacuum applied. We have used a thicker layer of CuPc to increase the measured intensity. Initial measurements were taken before gas dosage. Premixed 10 ppm of NO_2 or NH_3 in balance dry air from Linde Gas Singapore was then released into the measurement chamber, with an outlet to prevent build-up of the respective gas in the chamber. The data presented are an average of over 10 scans, and all data have been corrected to the signal of Cu foil to offset any possible shift across the measurement. Fourier transformation was also performed to examine the interaction of Cu with its neighboring atoms and tested gases on the extended X-ray absorption fine structure (EXAFS) region, which has an accuracy of ∼0.01 Å for the bond length.[38]

DOI: 10.1021/acsomega.8b02108
ACS Omega 2019, 4, 10388−10395

RESULTS AND DISCUSSION

Sensing-Layer Characterization. The morphology of the deposited CuPc layers on blank substrates was characterized using AFM and shown in Figure 1, where the CuPc layers are

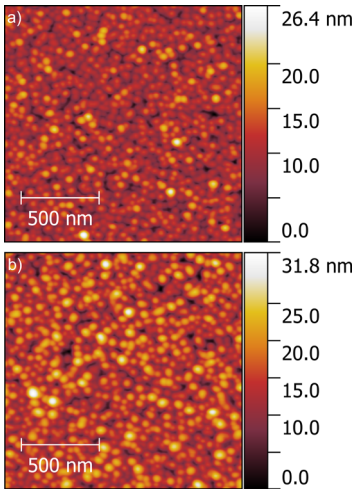

Figure 1. AFM images of (a) 100 and (b) 200 nm CuPc on blank Si/SiO_2 substrates.

comprised of grains growing normal to the substrate. Both 100 and 200 nm CuPc layers have similar packing density, and the root-mean-square roughness (R_{rms}) was found to be 2.96 and 4.31 nm, respectively for the layers. The grains of 200 nm CuPc layer can be observed to be bigger than its thinner counterpart (Figure 1).

Highly oriented crystal structure can be observed in the 100 and 200 nm CuPc layers, with a single XRD peak at 7.14° that is equivalent to the lattice spacing d = 12.4 Å (Figure 2). The

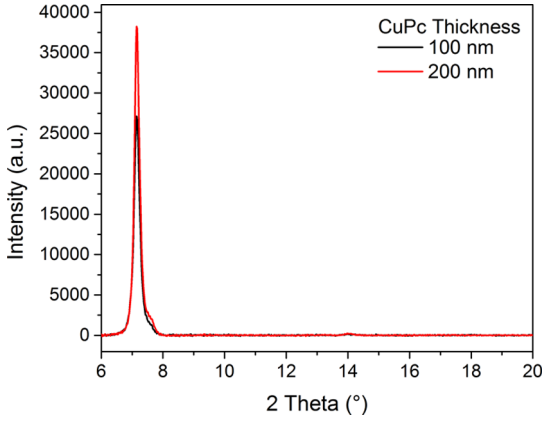

Figure 2. XRD patterns of 100 and 200 nm CuPc layers on blank substrates.

intensity of this single peak is also observed to be greater in 200 nm CuPc layer than in its 100 nm counterpart. The crystallinity in both samples is advantageous for reproducing XAS measurements, as will be described later.

CuPc layers (100 and 200 nm) were characterized using AFM and XRD. The main differences between these layers lie in bigger grains and higher crystallinity of the thicker layer, which is in agreement with previous works carried out in studying Pc layers of different thicknesses.[39,40] However, given that the differences between the two CuPc layers are less than two times, it is assumed that XAS measurements taken with 200 nm CuPc layer would be similar for 100 nm CuPc layer.

Gas Measurement. Chemiresistors with 100 nm CuPc deposited were dosed with varying concentrations of NO_2 or NH_3 in balance dry synthetic air. For each of the current measurement made at room temperature with a bias voltage of 5 V, fresh, pristine samples were used to prevent residual effects of previous NO_2 or NH_3 gas exposure.

Exposure of the CuPc chemiresistor to oxidizing gas NO_2 results in a positive change in the current, as shown in Figure 3a. On the other hand, negative current change was observed

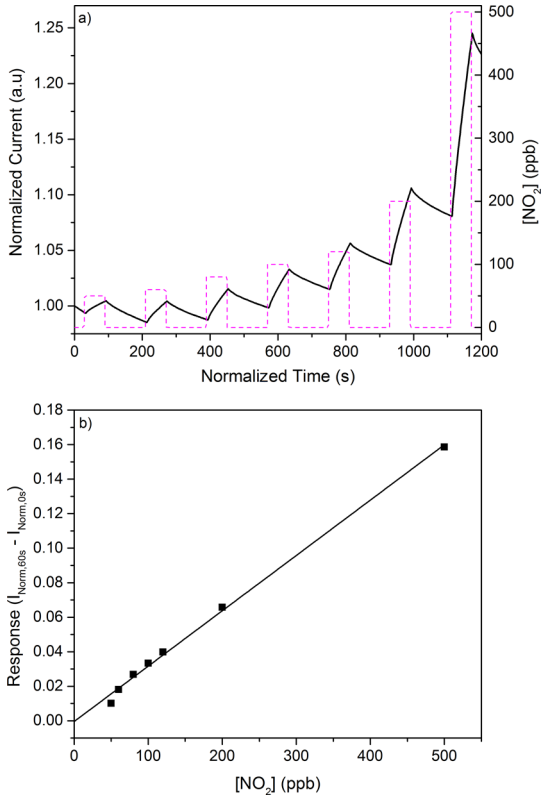

Figure 3. (a) Normalized measured current of chemiresistor with 100 nm CuPc sensing layer, as exposed to 50−500 ppb NO_2 with a balance dry synthetic air of 20% O_2 content. The measurement was taken with an applied voltage of 5 V at room temperature, and the current was normalized to the start of the second dosing cycle. (b) Response against [NO_2] plot, as calculated from the normalized current.

when the pristine CuPc chemiresistors were exposed to varying concentrations of reducing gas NH_3 (Figure 4a). The current of the chemiresistors also does not recover fully to the pre-exposure level after 120 s, as seen in both Figures 3 and 4. By comparing the response of CuPc chemiresistors to either gas, an opposite current change upon gas exposure is due to the gas properties, that is, oxidizing and reducing gases. In exposing CuPc chemiresistors to either gas, the current changes linearly with the target gas concentration, as seen in Figures 3b and 4b. The chemiresistors also displayed a lower current change, and hence lower sensitivity to NH_3 than NO_2, even though higher NH_3 concentrations were used. This is reflected in the repeated measurements made to obtain the average sensitivity of CuPc chemiresistors to NO_2 or to NH_3 (Table 1). Specifically, 5 pristine chemiresistors were used for each gas,

DOI: 10.1021/acsomega.8b02108
ACS Omega 2019, 4, 10388−10395

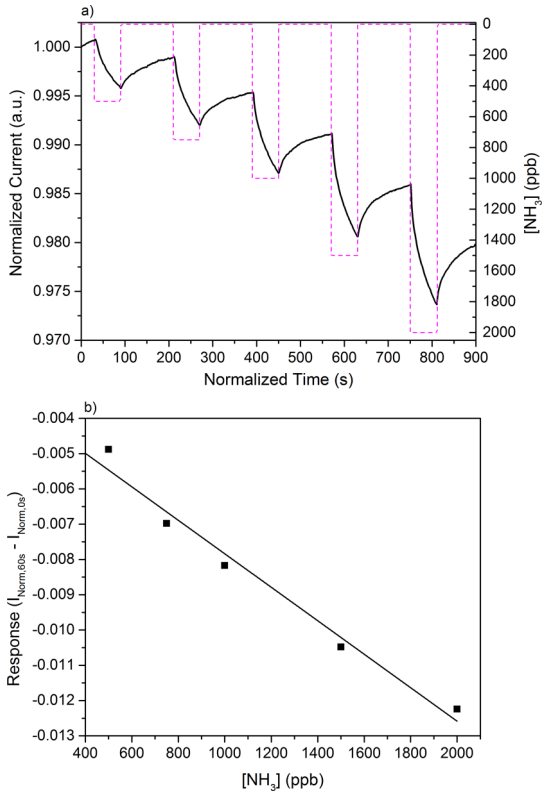

Figure 4. (a) Normalized measured current of chemiresistor with 100 nm CuPc sensing layer, as exposed to 500−2000 ppb NH_3 with balance dry synthetic air of 20% O_2 content. The measurement was taken with an applied voltage of 5 V at room temperature. (b) Response against [NH_3] plot, as calculated from the normalized current.

Table 1. Average Gas Sensitivity Based on 10 CuPc Chemiresistors of 100 nm to NO_2 or to NH_3 with the Respective Standard Deviation[a]

target gas	average sensitivity (10^{-4})	standard deviation (10^{-6})
NO_2	3.41	8.26
NH_3	−0.043	0.48

[a]Sensitivity is derived from the gradient of the response against concentration plot from each chemiresistor.

resulting in a total of 10 chemiresistors used. The gradient from the response against concentration plot, such as Figures 3b and 4b, was taken as the sensitivity.

Sensing Mechanism and Interaction. Positive and negative current changes observed in the CuPc chemiresistors because of exposure to NO_2 or to NH_3, respectively, can be attributed to the electron transfer between the gas and CuPc sensing layer. In particular, the electron transfer from CuPc to NO_2 has been reported to form holes in CuPc, leading to the increase in current of the p-type CuPc sensing layer.[33,41] On the other hand, the electron donation from the NH_3 gas to CuPc results in the depletion of holes, thereby reducing the current, as seen in our results. Although the observations of the changes in the measured current of CuPc devices as exposed to NO_2 or NH_3 can be explained to be because of the electron transfer, the interaction sites at the macrocycle or metal center have not been clarified. Prior to the determination of the interaction site, the bonding characteristics of CuPc will be first discussed.

In CuPc, the Cu atom is coordinate bonded to the Pc macrocycle, leading to hybridization of the orbitals of Cu and Pc macrocycle. Consequently, the highest occupied molecular orbital (HOMO) and lowest unoccupied molecular orbital (LUMO) were found to be a_{1u} (π) and 2_{eg} (π^*) orbitals respectively, with a Pc macrocycle character.[32] It should be noted that for the HOMO and LUMO of MPc, higher metal character is possible, that is in FePc. In the case of MPc HOMO, as the d orbitals are filled up across the period, the metal 1_{eg} d orbital can be found lower in energy, leading to less metal character.[32] As a result, CuPc HOMO and LUMO have mainly a Pc macrocycle character because of its almost-filled d orbital. Subsequently, it is expected that in the interaction of CuPc sensing layer with NO_2 or NH_3, the Pc macrocycle will be involved. However, we would like to reiterate that there is a lack of consensus or agreement in the interaction site between the tested gas with CuPc in literature so far.

Without considering the frontier orbitals of CuPc, there are four possible interaction sites, such as on the pyrrole, bridging N atom or benzo moiety of Pc macrocycle, as well as on the axial of Cu atom. Upon interaction of CuPc with the gas analyte, there are not only electrical changes but also chemophysico changes, such as a change in the bond distance. In the XAS measurements of Cu atoms with its neighboring atoms, normalized Cu K-edge X-ray absorption near-edge structure (XANES) measurement of pristine 200 nm CuPc layer on blank substrate before and after exposure to NO_2 or to NH_3 are monitored, as shown in Figure 5. Pristine samples that have only been exposed to environmental air were used for each test, and any drift was corrected by using the reference Cu foil.

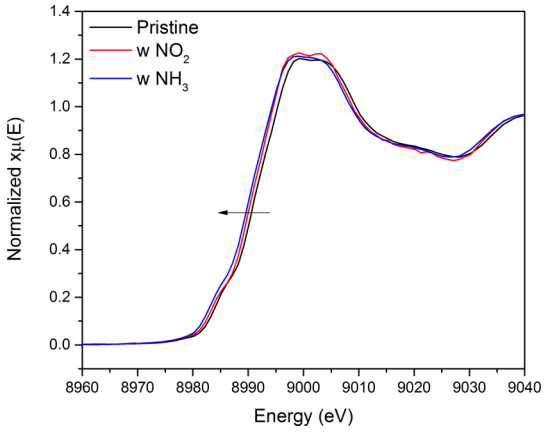

Figure 5. Normalized Cu K-edge XANES of pristine 200 nm CuPc on blank substrate before and during exposure to NO_2 or to NH_3.

It has been established in various research work that CuPc has a square planar structure with D_{4h} configuration.[32,42] Subsequently, a lack of features at the pre-edge and rising edge of the XANES of the pristine CuPc sample (Figure 5) can be obtained because of this centrosymmetric structure.[43,44] Upon exposure to low concentrations of NO_2 or NH_3, a left shift in the rising edge can be seen. Although such shift is typically linked to a change in oxidation state, a change in the molecular structure or orbital overlap with bonded ligands may also cause such a shift.[45−47] In our case, it may be deduced that there is a reduction in Cu^{2+} of CuPc, but the left shift seen in our results could also be because of the change in the CuPc structure from square planar, as well as hybridization of ligands with Cu d-

DOI: 10.1021/acsomega.8b02108
ACS Omega 2019, 4, 10388−10395

orbitals. Although the nature of the shift will be further discussed below, the left shift observed in XANES in Figure 5 verified the existence of an interaction between CuPc and the gas (NO_2 or NH_3).

From the first derivative (Figure 6) of the normalized XANES in Figure 5, an ca. 5 eV shift from the elemental Cu K-edge with an energy of 8979 eV shows the +2 oxidation state of the CuPc layer.[43,48] It is noted that the rising edge, ca. 8984 eV, of pristine CuPc layer here is similar to the reported value of CuPc layer that was deposited using glow discharge sublimation method.[49] In Figure 6, two main peaks labeled as peak A and peak B were obtained and can be correlated with 1s → 4p transition. Furthermore, details on the distortion from ligands bonded on axial position can be derived from peak A.[43,50] In our case, the distortion because of ligands in axial position of Cu in CuPc is inferred to be low, given the low intensity of peak A in all three spectra.

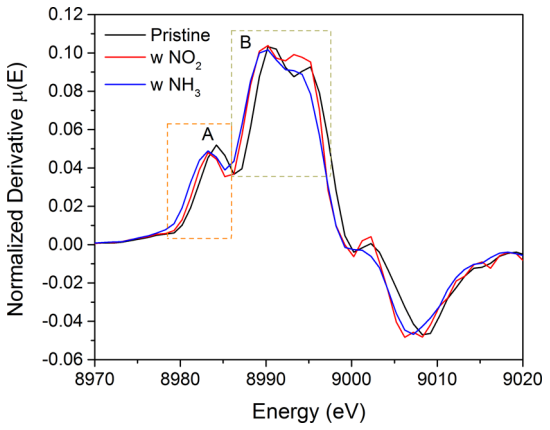

Figure 6. First derivative of normalized XANES of 200 nm CuPc before exposure to target gas (pristine) and during exposure to NO_2 or to NH_3 with peak A and B relating to the 1s → 4p transition.

Fourier-transformed EXAFS of CuPc layer before and during gas exposure is shown in Figures 7 and 8 for NO_2 and NH_3, respectively. The first major peak in both figures represents the shortest bond between Cu metal center with its neighboring atoms, and in CuPc, this is the Cu−N bond formed between the metal center and the macrocycle. In Figure 7, a left shift, ca 0.03 Å, toward shorter Cu−N bond can be observed during the exposure of the layer to NO_2. On the other hand, there is a lack of such shift in CuPc upon exposure to NH_3 (Figure 8). A repeated measurement with fresh, pristine CuPc layer to validate the results seen in Figures 7 and 8 is shown in Figures S1−S3.

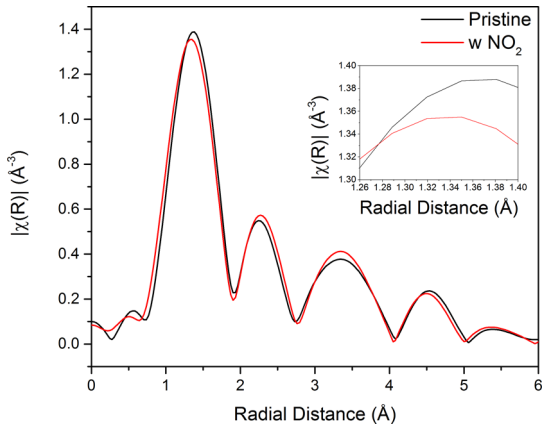

Figure 7. Fourier-transformed EXAFS of pristine 200 nm CuPc before and during NO_2 exposure.

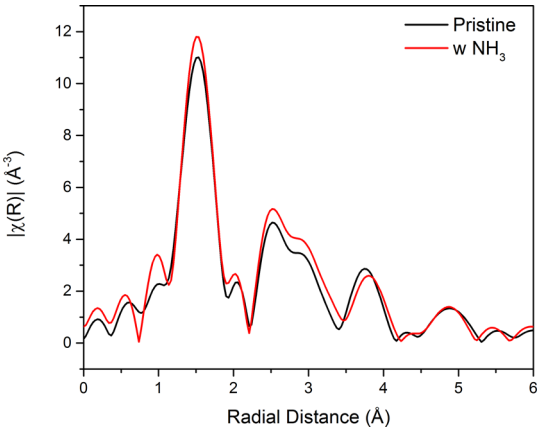

Figure 8. Fourier-transformed EXAFS of pristine 200 nm CuPc before and during NH_3 exposure.

The XAS measurement results shown here indicate that the interaction between CuPc and the gas (NO_2 or NH_3) does not occur at the Cu metal center but on the macrocycle instead. A first indication is seen in the similar intensity of peak A in the first derivative of XANES (Figure 6) in all three spectra because of low distortion from axial ligands or even the lack of it. Furthermore, the coordination of NO_2 onto the axial position of CuPc should theoretically result in a Cu−NO_2 or Cu−ONO bond, that is, 0.01−0.04 Å longer than Cu−N bond.[51] On the other hand, by referencing from the study done using ZnPc with analytes such as NH_3,[52] an elongation of the Cu−N(Pc macrocycle) bond can be expected from the interaction of the gas on the metal center. ZnPc and CuPc have comparable frontier orbitals and are thus suitable as a point of reference here. In view that there is a lack of such Cu−N elongation in our results, which can be seen by a right shift in EXAFS, or an additional shoulder peak on the Cu−N peak, this suggests that there is a lack of axial coordination of NO_2 or NH_3 on the metal center.

On the other hand, the shortening of Cu−N bond upon exposure to NO_2, as presented in EXAFS (Figure 7 and repeated in Figures S1 and S2), could be because of the interaction of CuPc with NO_2 on the macrocycle, in particular, on the pyrrole moiety. In the interaction on the pyrrole moiety of CuPc, the Cu−N bond is compressed so as to accommodate the NO_2 gas molecule, as shown in Figure 9. This proposition of interaction at the Pc macrocycle can be supported by looking at the molecular orbitals of CuPc and NO_2, where the electron transfers from CuPc HOMO, which is a_{1u} π orbital of Pc macrocycle to 4_{a1} π orbital of NO_2.[32,42] It should be noted that it may be possible for additional interaction between these π orbitals, given that the CuPc LUMO and HOMO of NO_2^- are of π character.[42,53]

For the interaction of CuPc with NH_3, based on the first derivative of XANES, it is also proposed to be on the Pc macrocycle. This is substantiated by looking into the molecular orbital of CuPc and NH_3. Here, the electron transfers from NH_3 nonbonding π orbital to CuPc LUMO of π Pc macrocycle orbital.[55,56] However, in contrast to the interaction of CuPc with NO_2, the interaction of CuPc with NH_3 is proposed to be

DOI: 10.1021/acsomega.8b02108
ACS Omega 2019, 4, 10388−10395

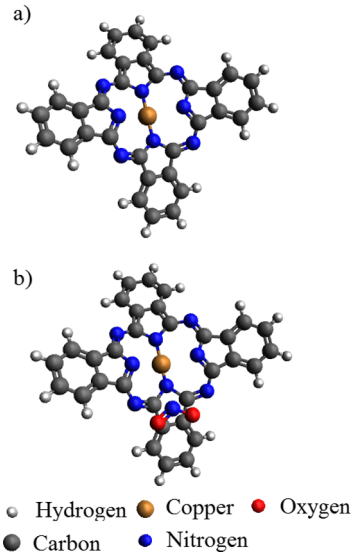

Figure 9. Illustration of (a) CuPc molecule and (b) subsequent Cu−N bond shortening in CuPc molecule upon interaction with one NO_2 molecule. Drawn using Avogadro.[54]

either on the benzo moiety or bridging atom because of the lack of obvious shift in Cu−N bond in both experiments (Figures 8, S1, and S3). It should be noted that our proposition here contradicts works that support a metal center interaction,[33] as well as π-back donation,[52] which we do not expect of CuPc HOMO (πa_{1u}) to LUMO of NH_3 (σ^*).[55,56]

On the basis of the in situ XAS measurements coupled with frontier molecular orbitals information, the interaction of CuPc with NO_2 or NH_3 has been reasonably justified to be on the Pc macrocycle. This interaction thus leads to a slight deviation of the CuPc square planar structure, which was reflected in the left shift of the XANES spectra (Figure 5). The electron transfer from NH_3 or additional π-interaction between NO_2 and CuPc may also contribute to this left shift, which reflects as a decrease in the contribution of Cu to the electron density of CuPc. For future work, it will be interesting to investigate the gas interaction of CuPc by making in situ N K-edge measurements, although there are challenges because of the compromise of ultrahigh vacuum (UHV) condition upon injection of gas for in situ measurements. In particular, N K-edge will require UHV conditions because of the low energies involved.

CONCLUSIONS

The gas sensitivity of CuPc to NO_2 and NH_3 was evaluated and showed an increase and decrease in the measured current, respectively, upon gas exposure. The interaction site was investigated using in situ XAS, an operando approach to investigate the chemical environment of the neighboring atoms of the target Cu metal center in this work.

Using XANES, a left shift in the spectra upon gas exposure because of a slight loss of centrosymmetricity of CuPc indicates the interaction of the respective gases with CuPc. The first derivative of XANES also suggests low or a lack of axial position coordination on the Cu metal center. On the other hand, the interaction on the macrocycle is supported by the EXAFS. For instance, from the EXAFS of CuPc with NO_2, the presence of a left shift of the Cu−N peak, rather than a right shift, indicates a compression of the Cu−N (Pc macrocycle) and, subsequently, suggests that the interaction is at the pyrrole moiety of the Pc macrocycle rather than on the metal center. The interaction of NH_3 with CuPc can be seen in the left shift of XANES, and it is proposed that the interaction can be on the benzo moiety or bridging atom because of the lack of obvious shifts in EXAFS. Our proposition here is in tandem with the molecular orbital information of CuPc, NO_2, and NH_3. In summary, interaction sites for gas interaction analysis were demonstrated in this work using CuPc with the oxidizing gas NO_2 and reducing gas NH_3.

ASSOCIATED CONTENT

Supporting Information

The Supporting Information is available free of charge on the ACS Publications website at DOI: 10.1021/acsomega.8b02108.

Repeated XAS measurement on a pristine CuPc layer as well as fitting of EXAFS of the respective measurements (PDF)

AUTHOR INFORMATION

Corresponding Author

*E-mail: pslee@ntu.edu.sg (P.S.L.).

ORCID

Liping Sharon Chia: 0000-0003-4703-7815
Yong Hua Du: 0000-0003-2655-045X
Pooi See Lee: 0000-0003-1383-1623

Author Contributions

All authors have given approval to the final version of the manuscript.

Notes

The authors declare no competing financial interest.

ACKNOWLEDGMENTS

This work was supported by the Singapore Economic Development Board (EDB), Nanyang Technological University (NTU) School of Materials Science and Engineering and Robert Bosch (SEA) Pte Ltd through the EDB-Industrial Postgraduate Programme.

ABBREVIATIONS

AFM, atomic force microscopy; CuPc, copper phthalocyanine; EXAFS, extended X-ray absorption fine structure; MFC, mass flow controller; MO_x, metal oxide; MPc, metal phthalocyanine; NIOSH, National Institute for Occupational Safety and Health; P3HT, poly-3-hexylthiophene; PLC, programmable logic controller; REL, recommended exposure limit; SSLS, Singapore Synchrotron Light Source; UHV, ultrahigh vacuum; WHO, World Health Organization; XAS, X-ray absorption spectroscopy; XANES, X-ray absorption near-edge structure

REFERENCES

(1) Jarvis, D. J.; Adamkiewicz, G.; Heroux, M.-E.; Rapp, R.; Kelly, F. J. Nitrogen dioxide. In *WHO Guidelines for Indoor Air Quality: Selected Pollutants*; World Health Organization: Geneva, 2010.

(2) Richter, A.; Burrows, J. P.; Nüß, H.; Granier, C.; Niemeier, U. Increase in tropospheric nitrogen dioxide over China observed from space. *Nature* **2005**, *437*, 129−132.

(3) Brunekreef, B.; Holgate, S. T. Air pollution and health. *The Lancet* **2002**, *360*, 1233−1242.

DOI: 10.1021/acsomega.8b02108
ACS Omega 2019, 4, 10388−10395

(4) World Health Organization. *Health Aspects of Air Pollution with Particulate Matter, Ozone and Nitrogen Dioxide*: Report on a WHO working group: Bonn, Germany, Jan 13−15, 2003.
(5) Orehek, J.; Massari, J. P.; Gayrard, P.; Grimaud, C.; Charpin, J. Effect of short-term, low-level nitrogen dioxide exposure on bronchial sensitivity of asthmatic patients. *J. Clin. Invest.* **1976**, *57*, 301−307.
(6) *NIOSH Pocket Guide to Chemical Hazards*. https://www.cdc.gov/niosh/npg/npgd0454.html (accessed June 27, 2017).
(7) Behera, S. N.; Sharma, M.; Aneja, V. P.; Balasubramanian, R. Ammonia in the atmosphere: a review on emission sources, atmospheric chemistry and deposition on terrestrial bodies. *Environ. Sci. Pollut. Res.* **2013**, *20*, 8092−8131.
(8) Timmer, B.; Olthuis, W.; van den Berg, A. Ammonia sensors and their applications-a review. *Sens. Actuators, B* **2005**, *107*, 666−677.
(9) Committee, N. R. C. U. Ammonia Acute Exposure Guideline Levels. In *Acute Exposure Guideline Levels for Selected Airborne Chemicals*; National Academies Press: Washington DC, US, 2008; Vol. *6*.
(10) Zhu, X.; Burger, M.; Doane, T. A.; Horwath, W. R. Ammonia oxidation pathways and nitrifier denitrification are significant sources of N2O and NO under low oxygen availability. *Proc. Natl. Acad. Sci.* **2013**, *110*, 6328−6333.
(11) Righettoni, M.; Amann, A.; Pratsinis, S. E. Breath analysis by nanostructured metal oxides as chemo-resistive gas sensors. *Mater. Today* **2015**, *18*, 163−171.
(12) Comini, E.; Faglia, G.; Sberveglieri, G.; Pan, Z.; Wang, Z. L. Stable and highly sensitive gas sensors based on semiconducting oxide nanobelts. *Appl. Phys. Lett.* **2002**, *81*, 1869−1871.
(13) Marquis, B. T.; Vetelino, J. F. A semiconducting metal oxide sensor array for the detection of NOx and NH3. *Sens. Actuators, B* **2001**, *77*, 100−110.
(14) Zeng, J.; Hu, M.; Wang, W.; Chen, H.; Qin, Y. NO2-sensing properties of porous WO3 gas sensor based on anodized sputtered tungsten thin film. *Sens. Actuators, B* **2012**, *161*, 447−452.
(15) Nanto, H.; Minami, T.; Takata, S. Zinc-oxide thin-film ammonia gas sensors with high sensitivity and excellent selectivity. *J. Appl. Phys.* **1986**, *60*, 482−484.
(16) Zhang, D.; Liu, Z.; Li, C.; Tang, T.; Liu, X.; Han, S.; Lei, B.; Zhou, C. Detection of NO2down to ppb Levels Using Individual and Multiple In2O3Nanowire Devices. *Nano Lett.* **2004**, *4*, 1919−1924.
(17) Zhang, J.; Liu, X.; Neri, G.; Pinna, N. Nanostructured Materials for Room-Temperature Gas Sensors. *Adv. Mater.* **2015**, *28*, 795−831.
(18) Liu, S.; Yu, B.; Zhang, H.; Fei, T.; Zhang, T. Enhancing NO2 gas sensing performances at room temperature based on reduced graphene oxide-ZnO nanoparticles hybrids. *Sens. Actuators, B* **2014**, *202*, 272−278.
(19) Liu, Y.; Jiao, Y.; Zhang, Z.; Qu, F.; Umar, A.; Wu, X. Hierarchical SnO2 Nanostructures Made of Intermingled Ultrathin Nanosheets for Environmental Remediation, Smart Gas Sensor, and Supercapacitor Applications. *ACS Appl. Mater. Interfaces* **2014**, *6*, 2174−2184.
(20) Ammu, S.; Dua, V.; Agnihotra, S. R.; Surwade, S. P.; Phulgirkar, A.; Patel, S.; Manohar, S. K. Flexible, All-Organic Chemiresistor for Detecting Chemically Aggressive Vapors. *J. Am. Chem. Soc.* **2012**, *134*, 4553−4556.
(21) Kong, J.; Franklin, N. R.; Zhou, C.; Chapline, M. G.; Peng, S.; Cho, K.; Dai, H. Nanotube Molecular Wires as Chemical Sensors. *Science* **2000**, *287*, 622−625.
(22) Li, J.; Lu, Y.; Ye, Q.; Cinke, M.; Han, J.; Meyyappan, M. Carbon Nanotube Sensors for Gas and Organic Vapor Detection. *Nano Lett.* **2003**, *3*, 929−933.
(23) Mabeck, J. T.; Malliaras, G. G. Chemical and biological sensors based on organic thin-film transistors. *Anal. Bioanal. Chem.* **2006**, *384*, 343−53.
(24) Liao, F.; Chen, C.; Subramanian, V. Organic TFTs as gas sensors for electronic nose applications. *Sens. Actuators, B* **2005**, *107*, 849−855.
(25) Matindoust, S.; Farzi, A.; Baghaei Nejad, M.; Shahrokh Abadi, M. H.; Zou, Z.; Zheng, L.-R. Ammonia gas sensor based on flexible polyaniline films for rapid detection of spoilage in protein-rich foods. *J. Mater. Sci.: Mater. Electron.* **2017**, *28*, 7760−7768.
(26) Agbor, N. E.; Petty, M. C.; Monkman, A. P. Polyaniline thin films for gas sensing. *Sens. Actuators, B* **1995**, *28*, 173−179.
(27) Collins, R. A.; Mohammed, K. A. Gas sensitivity of some metal phthalocyanines. *J. Phys. D: Appl. Phys.* **2000**, *21*, 154.
(28) Newton, M. I.; Starke, T. K. H.; McHale, G.; Willis, M. R. The effect of NO2 doping on the gas sensing properties of copper phthalocyanine thin film devices. *Thin Solid Films* **2000**, *360*, 10−12.
(29) Guillaud, G.; Simon, J.; Germain, J. P. Metallophthalocyanines. *Coord. Chem. Rev.* **1998**, *178−180*, 1433−1484.
(30) Dong, Z.; Kong, X.; Wu, Y.; Zhang, J.; Chen, Y. High-sensitive room-temperature NO 2 sensor based on a soluble n-type phthalocyanine semiconductor. *Inorg. Chem. Commun.* **2017**, *77*, 18−22.
(31) Zan, L.; WenRui, J.; Xiaohong, W.; Yunbo, S. Preparation and Characterization of Novel Octa-iso-Pentyloxymetallophthalocyanines (M = Pb, Ni, Cu) Gas Sensors. *Int. J. Electrochem. Sci.* **2013**, *8*, 7044−7052.
(32) Liao, M.-S.; Scheiner, S. Electronic structure and bonding in metal phthalocyanines, Metal = Fe, Co, Ni, Cu, Zn, Mg. *J. Chem. Phys.* **2001**, *114*, 9780−9791.
(33) Basova, T.; Kol'tsov, E.; Igumenov, I. Spectral investigation of interaction of copper phthalocyanine with nitrogen dioxide. *Sens. Actuators, B* **2005**, *105*, 259−265.
(34) Lozzi, L.; Picozzi, S.; Santucci, S.; Cantalini, C.; Delley, B. Photoemission and theoretical investigations on NO2 doping of copper phthalocyanine thin films. *J. Electron Spectrosc. Relat. Phenom.* **2004**, *137−140*, 101−105.
(35) Yano, J.; Yachandra, V. K. X-ray absorption spectroscopy. *Photosynth. Res.* **2009**, *102*, 241−254.
(36) Ciston, J.; Si, R.; Rodriguez, J. A.; Hanson, J. C.; Martínez-Arias, A.; Fernandez-García, M.; Zhu, Y. Morphological and Structural Changes during the Reduction and Reoxidation of CuO/CeO2 and Ce1-xCuxO2 Nanocatalysts: In Situ Studies with Environmental TEM, XRD, and XAS. *J. Phys. Chem. C* **2011**, *115*, 13851−13859.
(37) Du, Y.; Zhu, Y.; Xi, S.; Yang, P.; Moser, H. O.; Breese, M. B. H.; Borgna, A. XAFCA: a new XAFS beamline for catalysis research. *J. Synchrotron Radiat.* **2015**, *22*, 839−843.
(38) Du, Y.; Wang, J.-o.; Jiang, L.; Borgna, L. S.; Wang, Y.; Zheng, Y.; Hu, T. Data analysis method to achieve sub-10 pm spatial resolution using extended X-ray absorption fine-structure spectroscopy. *J. Synchrotron Radiat.* **2014**, *21*, 756−761.
(39) Chia, L. S.; Palale, S.; Lee, P. S. Thickness-dependent sensitivity of Copper Phthalocyanine chemiresistive Nitrogen Dioxide sensors. In *IEEE Sensors*, Oct 30 to Nov 3, 2016.
(40) Lee, Y.-L.; Sheu, C.-Y.; Hsiao, R.-H. Gas sensing characteristics of copper phthalocyanine films: effects of film thickness and sensing temperature. *Sens. Actuators, B* **2004**, *99*, 281−287.
(41) Trogler, W. C. Chemical Sensing with Semiconducting Metal Phthalocyanines. In *Molecular Electronic Structures of Transition Metal Complexes I*; Mingos, D. M. P., Day, P., Dahl, J. P., Eds.; Springer Berlin Heidelberg: Berlin, Heidelberg, 2012; pp 91−117.
(42) Lever, A. B. P.; Pickens, S. R.; Minor, P. C.; Licoccia, S.; Ramaswamy, B. S.; Magnell, K. Charge-transfer spectra of metallophthalocyanines: correlation with electrode potentials. *J. Am. Chem. Soc.* **1981**, *103*, 6800−6806.
(43) Gaur, A.; Shrivastava, B. D.; Srivastava, K.; Prasad, J.; Singh, S. K. XAFS investigations of copper(II) complexes with tetradentate Schiff base ligands. *X-Ray Spectrom.* **2012**, *41*, 384−392.
(44) Chaboy, J.; Muñoz-Páez, A.; Carrera, F.; Merkling, P.; Marcos, E. S. Ab initio x-ray absorption study of copper K-edge XANES spectra in Cu(II) compounds. *Phys. Rev. B: Condens. Matter Mater. Phys.* **2005**, *71*, 134208.
(45) Shimizu, K.-i.; Maeshima, H.; Yoshida, H.; Satsuma, A.; Hattori, T. Ligand field effect on the chemical shift in XANES spectra of Cu(II) compounds. *Phys. Chem. Chem. Phys.* **2001**, *3*, 862−866.
(46) Tromp, M.; Moulin, J.; Reid, G.; Evans, J. Cr K-Edge XANES Spectroscopy: Ligand and Oxidation State Dependence — What is

DOI: 10.1021/acsomega.8b02108
ACS Omega 2019, 4, 10388−10395

Oxidation State?. *AIP Conference Proceedings*, 2007; Vol. *882*, pp 699−701.
(47) Tomson, N. C.; Williams, K. D.; Dai, X.; Sproules, S.; DeBeer, S.; Warren, T. H.; Wieghardt, K. Re-evaluating the Cu K pre-edge XAS transition in complexes with covalent metal-ligand interactions. *Chem. Sci.* **2015**, *6*, 2474−2487.
(48) Joseph, D.; Basu, S.; Jha, S. N.; Bhattacharyya, D. Chemical shifts of K-X-ray absorption edges on copper in different compounds by X-ray absorption spectroscopy (XAS) with Synchrotron radiation. *Nucl. Instrum. Methods Phys. Res., Sect. B* **2012**, *274*, 126−128.
(49) Maggioni, G.; Carturan, S.; Tonezzer, M.; Bonafini, M.; Vomiero, A.; Quaranta, A.; Maurizio, C.; Giannici, F.; Scandurra, A.; D'Acapito, F.; Della Mea, G.; Puglisi, O. Effects of Heat Treatments on the Properties of Copper Phthalocyanine Films Deposited by Glow-Discharge-Induced Sublimation. *Chem. Mater.* **2006**, *18*, 4195−4204.
(50) Gaur, A.; Klysubun, W.; Soni, B.; Shrivastava, B. D.; Prasad, J.; Srivastava, K. Identification of different coordination geometries by XAFS in copper(II) complexes with trimesic acid. *J. Mol. Struct.* **2016**, *1121*, 119−127.
(51) Rousseau, R.; Ozarowski, A.; Aroca, R.; de A. Soares, L.; Trsic, M. The electronic structure of metallated phthalocyanine-NO2 adducts. *J. Mol. Struct.* **1994**, *317*, 287−297.
(52) Saini, G. S. S.; Singh, S.; Kaur, S.; Kumar, R.; Sathe, V.; Tripathi, S. K. Zinc phthalocyanine thin film and chemical analyte interaction studies by density functional theory and vibrational techniques. *J. Phys.: Condens. Matter* **2009**, *21*, 225006.
(53) Burnelle, L.; Beaudouin, P.; Schaad, L. J. Electronic structure of nitrogen dioxide, its ions, and its dimer. *J. Phys. Chem.* **1967**, *71*, 2240−2247.
(54) Hanwell, M. D.; Curtis, D. E.; Lonie, D. C.; Vandermeersch, T.; Zurek, E.; Hutchison, G. R. Avogadro: An advanced semantic chemical editor, visualization, and analysis platform. *J. Cheminform.* **2012**, *4*, 17.
(55) Stöhr, J. Symmetry and Molecular Orbitals. In *NEXAFS Spectroscopy*; Springer Berlin Heidelberg: Berlin, Heidelberg, 1992; pp 48−78.
(56) Miessler, G. L.; Fischer, P. J.; Tarr, D. A. Molecular Orbitals. In *Inorganic Chemistry*, 5th ed.; Pearson: Boston, 2014; pp 117−168.

DOI: 10.1021/acsomega.8b02108
ACS Omega 2019, 4, 10388−10395